Electrocatalysis (2017) 8:565–576
DOI 10.1007/s12678-017-0368-8

ORIGINAL ARTICLE

Fates of Hydrogen During Alumina Growth Below Yttria Nodules in FeCrAl(RE) at Low Partial Pressures of Water

Vedad Babic[1] · **Christine Geers**[1] · **Bo Jönsson**[1,2] · **Itai Panas**[1]

Published online: 16 March 2017

Abstract Oxidation of FeCrAl(Re), when exposed to ~35 ppm of water as sole supply of oxygen in predominantly nitrogen atmosphere, has two characteristic signatures. One is the internal nitridation owing to chromia nodules acting windows toward nitrogen permeation locally short-circuiting the protective α-Al_2O_3 scale. The second remarkable feature is the growth of thick, apparently defect-rich alumina scale under yttria-rich nodules. Hence, one part of the present study comprises exploratory DFT calculations to discriminate between the impacts of chromia and yttria viz. nitrogen permeation. The second part concerns boundary conditions for apparent rapid growth of alumina under yttria nodules. Yttria-associated surface energy stabilization of defect-rich alumina in presence of water was argued to involve hydrolysis-driven hydroxylation of said interface. Subsequent inward growth of the alumina scale was associated with outward diffusion of oxygen vacancies to be accommodated by the remaining proton producing a hydride ion upon surfacing at yttria-decorated alumina interfaces. The latter comprises the cathode process in a quasi-Wagnerian context. Two fates were discussed for this surface ion. One has H^-–H^+ recombination to form H_2 at the interface in conjunction with OH^- accommodation upon hydration, while the second allows hydrogen to be incorporated at V_O sites in hydroxylated grain boundaries of the growing alumina scale. The latter was taken to explain the experimentally observed rapid oxide growth under yttria-rich nodules. Space charge due to proton reduction was proposed to cause transient inward cationic drag.

Keywords High temperature alloy · FeCrAl · Yttria · Alumina · Oxidation by water · Hydride in oxide · Oxygen vacancy · Hydrogen evolution · Confinement effect · Defects · Oxide growth · Low partial pressure of oxygen · N_2 atmosphere · H_2 reducing conditions

Introduction

The fate of hydrogen is of central concern in solid oxide fuel cell applications [1]. Processes competing with the generic property of the solid electrolytes, i.e., as proton conductors, are essential for the efficiency and longevity of the cell. The Wagnerian decomposition of corrosion phenomena into anode and cathode processes [2–5] makes possible a conceptual transferability between the two technologically, highly relevant fields of research. Utilization of this analogy is realized in dual-atmosphere fuel cell interconnection, which has hydrogen permeation through the steel as an important process causing breakaway corrosion on the air side [6]. In the present study, the impact of low-partial pressures of water during oxidation of high-temperature alloys is taken to serendipitously offer an opportunity to explore the diverse roles of hydrogen in the oxidation process, while the main driving force in this endeavor is in fact the internal nitridation [7]. Indeed, very low oxygen activities in predominantly N_2(g) environment have unique corrosive impact at elevated temperatures. Alloys, which display near-ideal protective properties under normal corrosive conditions, suddenly exhibit surprising vulnerability. FeCrAl is one such alloy for which chromia particles of possible carbide origin embedded in α-Al_2O_3 scale were proven to short-circuit the protective oxide scale by offering a

✉ Itai Panas
itai@chalmers.se

[1] Department of Chemistry and Chemical Engineering, Chalmers University of Technology, SE-412 96 Göteborg, Sweden

[2] Sandvik Heating Technology AB, Hallstahammar, Sweden

window for nitrogen ingress, thus causing rapid internal nitridation and degradation. The detrimental impact of nitrogen once arriving at the oxide/alloy interface originates from its significant solubility in the alloy. This property distinguishes the N_2 atmosphere from, e.g., O_2/H_2O; in that, the low solubility of oxygen in FeCrAl is in fact an essential reason for its excellent performance under oxidizing conditions. The resulting internal nitridation of aluminum, avoided under oxidizing conditions, disallows outward aluminum diffusion to form a protective oxide scale, and this in turn has catastrophic impact on the alloy component.

While the driving force for the internal nitridation is the formation of stable aluminum nitride in the alloy, a necessary condition for this to happen in the first place is the existence of chromium ions occupying coordinatively unsaturated surface sites (CUSs) at the gas/oxide interface, where N_2 is able to dissociate [7]. Thus, it was demonstrated that internal nitridation can result from formation of transient chromium oxynitrides comprising solid solution of oxygen ions, nitride ions, and oxygen vacancies in the chromia matrix. Access to the alloy is achieved by co-diffusion of nitrogen and oxygen through the transient chromium oxynitride. This is triggered by the chromia particle becoming reduced due to aluminum oxidation in a metathesis reaction. Subsequently, the reduced chromia is reoxidized by nitrogen acting oxidant, resulting in the chromia effectively constituting a window for nitrogen permeation. Indeed, it was shown in [7] that coordinatively unsaturated Cr site CUSs on chromia are able to support N_2 reduction.

Improved long-term corrosion properties have been achieved by introducing additives such as zirconium and yttrium in the alloy enhancing transport in the resulting alumina oxide grain boundaries by single Zr^{4+} or Y^{3+} ion decoration [8]. Here, the initial impact of yttria particles on the corrosion process is addressed, i.e., prior to their dissolution. Thus, one objective of the present study is to provide experimental evidence and theoretical rationale for selective oxygen permeation associated to yttria particles penetrating the alumina scale, while simultaneously shutting the nitrogen out. Indeed, facilitated oxidation at the metal/oxide interface is observed, i.e., at a competitive pace when compared to the internal nitridation.

Microscopy reports (vide infra) formation of a defect-rich Al_2O_3 at the yttria/alloy interface, rendering this region a sustained sink for aluminum. Consequently, depletion of Al in the alloy in the vicinity of the yttria particles is observed to cause an AlN-free halo in spite of nearby chromium-rich particles.

Necessary prerequisites for sustaining any N_2 dissociation are explored here, arriving at the concentration of CUS at the gas/yttria interface as being the single most important condition for N_2 dissociation. Relevance of this condition is put in question when taking into account hydrolysis and rapid transport of water equivalents along the yttria/alumina rim. Such hydrolysis offers one possible means to mediate rapid supply of oxygen along the yttria/alumina interfaces, thus achieving the requested vanishing chemical potential gradient along said interface. This impact of water hydrolysis, stabilizing alumina surfaces [9–12] as well as assisting transformation between different crystal structures by hydrolysis at surfaces and interfaces, is well documented [13]. In particular, it is complementary to any rapid oxygen vacancy V_O migration through yttria, alumina, or along said interface.

Conceptual understanding is sought along the lines of Wagner theory of oxidation. This theory assumes rapid equilibration of reduction processes at oxygen/oxide interface and correspondingly anode processes at oxide/metal interface, while the net rate of oxide growth is determined by outward diffusion of cations, outward diffusion of electrons, and inward diffusion of oxygen ions. The resulting rate is owing to the oxygen chemical potential gradient across the barrier oxide, and thus, it is inversely proportional to the oxide thickness. Here, we assume that the cations are static and anion vacancies rendering the oxygen ion mobility and that electron transport is not rate limiting. A handy expression is thus arrived at

$$\Delta\mu = \frac{k_B T}{D C^0_{V_O}} J_O(X)\cdot X \tag{1}$$

where $C^0_{V_O}$ is the concentration of oxygen vacancies and D is their bulk diffusivity. This equation states that the current density of oxygen ions $J_O(X)$ is inversely proportional of the oxide thickness if the chemical potential difference $\Delta\mu$ across the oxide is a constant independent of thickness. Density functional theory is employed here to explain how the conditions for the quasi-isotropic inward growth of defect-rich Al_2O_3 in the vicinity of yttria nodules may be satisfied. Central characteristics of the cathode are at focus, i.e., its location within the oxide and the fate of cathode. Rapid equilibrations of oxygen chemical potential along the circumference of the yttria particle and also along the interface between alloy and defect-rich Al_2O_3 are implied from the microscopy here, thus jointly determining the Wagnerian chemical potential difference which drives the quasi-parabolic alumina growth.

Chemical potentials for oxygen vacancies and mobilities of charged and uncharged oxygen vacancies in yttria and alumina bulk as well as in thin slabs are employed to assess how proximity to an interface such as that between yttria and alumina impacts the mobility of oxygen vacancies. Crucial to our understanding of what controls oxygen vacancy diffusion is the destabilization of two Kohn-Sham states [14]. The state associated with the vacancy is mainly of metal origin and thus resembles states belonging to the conduction band. Inasmuch as the diffusion of the oxygen vacancy is equivalent to the counter-diffusion of an oxygen atom, the second state to be destabilized at the transition state is of valence band origin. The different occupations of the vacancy state, i.e., charged or uncharged, become decisive to the resulting activation energy for oxygen vacancy diffusion. Our quasi-Wagnerian QW scenario utilizes

the charged oxygen vacancies $V_O^{\cdot\cdot}$ in two ways. Firstly, they offer enhanced mobility, e.g., compared to oxygen diffusion channels which utilize interstitial lattice sites; secondly, they offer impurity states in the band gap for propagating electrons to the cathode. The QW channel is contrasted by the diffusion of neutral oxygen vacancies, i.e., where separation of electron transport and charged oxygen vacancy diffusion does not occur.

In addition, Wagner theory of oxidation when employing water as oxidant is conditioned by strategies for supply of protons and disposal hydrogen, commonly by H_2 evolution, resulting from the proton reduction. The impact of the confining yttria/alumina interface however is taken to suppress the cathodic hydrogen evolution reaction (cf. [15, 16]). It is the transient hydrogen incorporation in oxygen vacancies, i.e., as $H^{\cdot}@V_O^{\cdot\cdot}$, that is proposed to render the resulting alumina rapidly growing as well as defect rich. While moieties such as $H^{\cdot}@V_O^{\cdot\cdot}$ have been discussed previously in various oxides, experimental proof has been elusive [1, 17]. Here, however, it is proposed to take central stage. In principle, hydrogen may subsequently utilize oxygen vacancies as diffusion paths, resulting in hydrogen dissolution in the alloy matrix and possibly complementary hydride formation there, as an ultimate deposit of cathode product, thus sustaining the further oxidation of aluminum by water-associated oxygen. This way, contact is made with the internal nitridation owing to the oxidation of aluminum [7]. In case of the latter, reduction of nitrogen and inward drag of nitride ions utilize networks of oxygen vacancies in redox-active, chromia-rich nodules, offering window for corresponding internal nitridation (see Fig. 1).

Experiment

The nitridation experiments were performed at 900 °C in a N_2–5% H_2 gas mixture with approximately 16 ppm oxygen as impurity in the nitrogen gas. Equilibrating the oxygen impurity with hydrogen provides around 35 ppm steam as oxidizing species to the gas stream and an oxygen partial pressure of 10^{-23} bar. This amount renders yttria, alumina, and even chromia thermodynamically stable. The gas mixture was streamed into a horizontal tube furnace with a flow of 6.3 cm/min with a sufficient purging time before and after the heating to avoid oxygen levels above the impurity limit. The 15 × 15 × 2-mm coupons consisting of the high-temperature, creep-resistant alloy Kanthal APMT™ (see chemical composition in Table 1) was placed in the center of the heat constant zone for 1 week. After the experiments, the specimens underwent thorough investigations focusing on surface, scale, and internal corrosion species by using surface scanning electron microscopy (SEM) studies, when indicated coupled with focused ion beam (FIB) and cross sectioning, either manually via epoxy embedding, cutting, and polishing or via the broad ion beam (BIB) technique. Internal nitridation owing to N_2 dissociation on coordinatively unsaturated chromium sites in chromia and subsequent nitrogen permeation to the alloy/chromia interface via transient chromium oxynitrides was validated (cf. Fig. 1, middle image, and [7]). The present study concerns rapid growth of defect-rich alumina under

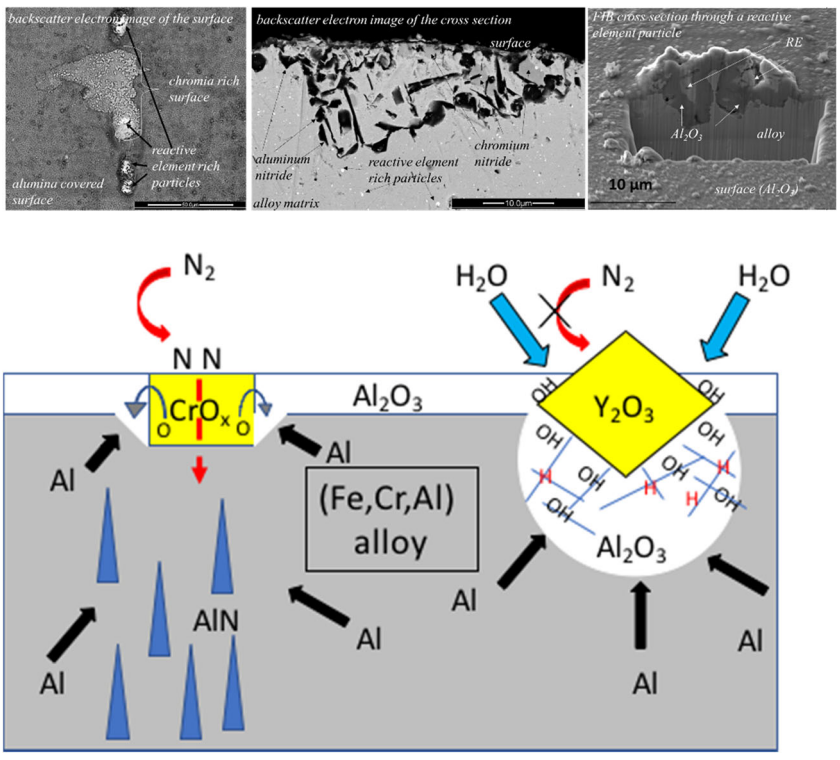

Fig. 1 *top* SEM images of Kanthal APMT™ specimen after exposure for 1 week. *left* Top view. *middle* Cross section through chromia nodule. *right* Cross section through yttria nodule. *bottom* Graphical representation of nitrogen penetration of chromia nodules and effective water penetration as hydroxides beneath yttria-rich nodules. In case of the latter, nitrogen is shut out and alumina formation is conditioned by disposal of hydrogen in the lattice or by hydrogen evolution

Table 1 Chemical composition of alloy Kanthal APMT

wt%	C	Si	Mn	Mo	Cr	Al	Fe	Other
Nominal				3.0	21.0	5.0	Balance	Y, N
Minimum	–	–	–		20.5			
Maximum	0.08	0.7	0.4		23.5	–		

nodules of the reactive element RE additive, i.e., yttria (cf. Fig. 1, right image).

Models

Fundamental to the present investigation is taking near-sightedness as point of departure in search for generic properties of defects in alumina and yttria. This means to say that for a sufficiently large unit cell, the local disorder of a defect-rich particle is well represented in spite of the crystalline setting inferred by the employed periodic boundary conditions. Two types of models are employed in our work, comprising bulk and slab models. The unit cell of yttria is taken to be cubic bixbyite with space group Ia-3 (no. 206). The unit cell consists of 48 Y and 72 O atoms. Alumina has corundum structure, the unit cell consists of 12 Al and 18 O atoms, and our bulk calculations employed 2 × 2 × 1 supercells (48 Al, 72 O). Slab models are formed by taking a unit/super cell of any material, choosing a surface along a given direction, and adding a vacuum slab on top of this surface to produce the sought interface. In our studies, the yttria slab consisted of the unit cell with a (100) surface and 10 Å of vacuum slab. The alumina slab on the other hand employed a 2 × 2 × 1 supercell with a (001) surface and 10-Å vacuum slab. The surfaces where the reactions were explored were designed to display all-O termination, half-O/half-metal ion, and all-metal ion termination.

The objectives were to explore

1. Any impact of extrinsic surface states on oxygen vacancy mobility in the immediate vicinity of a grain boundary,
2. Address oxygen coverage-dependent N_2 dissociation,
3. Impact of hydrolysis on surface stability,
4. Oxygen vacancy formation in bulk and relative stability at hydroxylated surface,
5. Fate of hydrogen on oxidation of aluminum by water.

See Fig. 2 for typical oxide slab models.

The impact of the said surface termination on transport-related properties was contrasted by that of completely hydroxylated interfaces—achieved by adding water molecules to the half-O/half-metal ion-terminated slab model in order to effectively remove said extrinsic states (see Fig. 3).

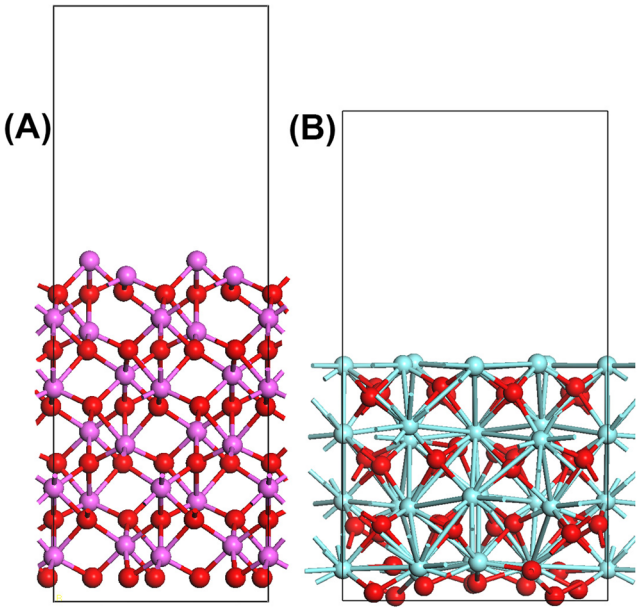

Fig. 2 Slab models of **a** a 2 × 2 × 1 supercell of corundum alumina with a (001) surface and 10-Å vacuum slab and **b** one unit cell of bixbyite yttria with a (100) surface and 10-Å vacuum slab. *Red* atoms are oxygen, *purple* aluminum, and *green* are yttrium. Both slabs offer 0% CUS coverage on one side and 100% CUS coverage on the other

In the "Surface Chemistry—Hydroxylation and Conditions for N_2 Dissociation" section, different interface terminations are compared as a means to (i) offer a ranking of their stabilities for further assessment regarding

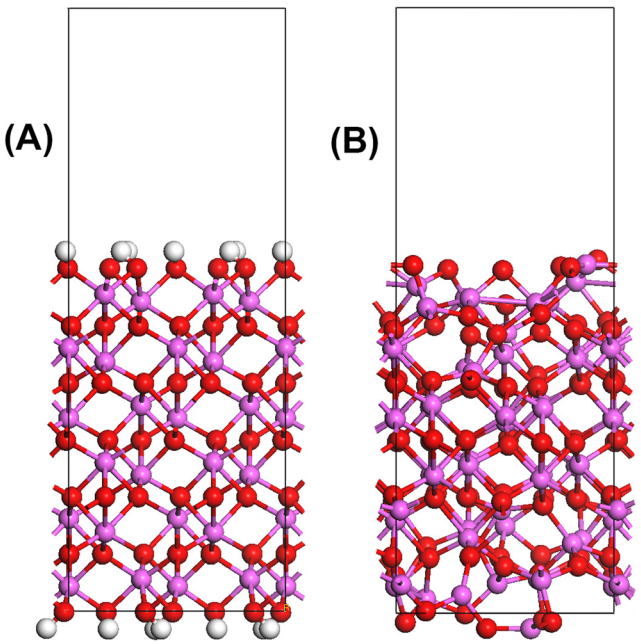

Fig. 3 **a** Slab model of a 2 × 2 × 1 supercell of corundum with a (001) surface which has been hydroxylated. **b** A slab model with a (001) surface which offers half-O/half-Al terminations on both sides. A 10-Å vacuum slab is added on top of the alumina layer in both cases. *Red* atoms are oxygen, *purple* aluminum, and *white* hydrogen. The geometries have been relaxed

how interface stabilities impact on properties of the interior of each of the slabs and (ii) contribute a consistency check by arriving at qualitative compatibilities. Only stoichiometric slabs are considered. The ranking is based on corresponding E_{surf} here defined as

$$\Delta E_{surf} = \frac{E_{slab} - nE_{bulk}}{2A} \quad (2)$$

that is the cost for forming the interfaces, n being the number of M_2O_3 formula units in the slab model. In case of hydroxylated interfaces, the relevant number becomes

$$\Delta E_{surf/OH} = \frac{E_{slab/OH} - (nE_{bulk} + mE_{H_2O})}{2A} \quad (3)$$

where m is the number of water molecules required for complete hydroxide terminations of both interfaces of the slab. The energies for free water molecules are taken as reference in the ranking. The purpose of the latter is to compare stabilities of hydroxide termination in contact with vacuum to the case when interfaces are allowed to form hydrogen bonds across the interface boundaries.

The first-principle calculations employed density functional theory [18] as realized in [19], utilizing the generalized gradient approximation (GGA) PBE function [20] in conjunction with ultrasoft pseudopotentials [21] as implemented in CASTEP [22]. The 550-eV cutoff energy was utilized. The Monkhorst-Pack scheme [23] with a 0.04-$Å^{-1}$ threshold was used for the k-point sampling, all being part of the Materials Studio computational platform [24].

Results and Discussion

In what follows, a contextual understanding based on first-principle calculations is sought for the observed quasi-isotropic buildup of apparently defect-rich alumina below yttria micro-domains as well as the absence of internal nitridation in their vicinity, both in contrast to chromia micro-domains co-existing with the yttria on said surface (cf. Fig. 1 again). Conceptually, the inward oxide growth of alumina is perceived here to involve a "stirring process" at the metal/oxide interface, which may be represented by a proportionation-disproportionation process. Upon proportionation, oxide growth occurs by the transient introduction of high concentrations of oxygen vacancies in the resulting defect-rich interface. Its sharpness is subsequently recovered by the diffusion of said oxygen vacancies away from the interface. Thus, while inward oxide growth is commonly understood as an inward transport of oxygen—and while equivalent—it is argued here that an outward diffusion of oxygen vacancies reflects better the causality of the corrosion process. The relevance of irregular defect-rich structures and grain boundaries in corrosion is underlined by the fact that creation of oxygen vacancies in bulk oxide is often virtually inaccessible, an exception to the rule offered by zirconium/zirconia system owing to the high solubility of oxygen in the metal [25, 26]. This is emphasized here by employing aluminum as oxygen sink to generate the oxygen vacancy, whereby Al_2O_3 is formed according to the reaction

$$M_{2X}O_{3X} + \frac{2}{3}Al \rightarrow M_{2X}O_{3X-1}(V_O) + \frac{1}{3}Al_2O_3 \quad (R1)$$

where M = Al, Y. Simulations show that the vacancy formation enthalpies are $\Delta H^{bulk}_{Y2O3}(V_O) = 1.53$ eV and $\Delta H^{bulk}_{Al203}(V_0) = 1.77$ when considering vacancy formation in bulk oxide.

Surface Chemistry—Hydroxylation and Conditions for N_2 Dissociation

In the experiment, the atmosphere consists of 95% N_2, 5% H_2 with ~35 ppm of H_2O, and where water acts sole oxygen source in the Al_2O_3 and Y_2O_3 formations. We may contrast formation of oxygen vacancies in bulk oxide to those formed at surfaces. In doing so, we note that the result is crucially dependent on the way that the surface is terminated. Indeed, any cleaving of a crystal to expose an atomic layer offering interface to a surrounding medium becomes truly ambiguous. Indeed, relevance of any such interface must be assessed on case-to-case basis. Here, extremal conditions are employed to address ability of yttria or alumina surfaces to support N_2 dissociation. While conditions for N_2 dissociation can be constructed, i.e., by exposing an entirely Y-terminated stoichiometric slab model, the justification of such a model must be put in question. Indeed, it was previously shown that the corresponding Al-terminated slab model was unable to support N_2 dissociation. Nevertheless, in what follows, the ability of yttria to support N_2 dissociation is discussed based on previous results for chromia [7]. Thus, for high N_2 concentration in the atmosphere, Geers et al. showed that chromia particles act as windows for nitrogen uptake into the alloy. This uptake is not found around yttria particles, the rationale for chromia supplying high concentrations of CUS on the reduced chromia surface, where nitrogen dissociation was owing to aluminum in the alloy acting reducing agent vis-à-vis the chromia. Similar studies of yttria employed a slab consisting of 48 Y and 72 O atoms. Oxygen surface coverages reflecting all-Y//all-O as well as half-Y/half-O terminations were employed. In contrast to alumina, results show that it is indeed possible

to adsorb and dissociate N_2 on the all-Y-terminated surface, $\Delta H_{ads}^{0\%} = -2.43$ eV and $\Delta H_{dis}^{0\%} = -1.13$ eV; i.e., the molecular chemisorption comes out more stable than the atomic. However, N_2 does not bind to a half-Y/half-O-covered surface. What discriminates Al and Y from Cr is the ability of the latter to display different oxidation states, i.e., Cr(II), Cr(III), and Cr(IV). In case of Y and Al, the +III oxidation state dominates. Finally, taking into consideration the absence of reducing agents for yttria and alumina, it is concluded that sufficient CUS coverage to facilitate the N_2 dissociation, necessary for the subsequent uptake, is not achieved.

In case of both yttria and alumina, the reduced crystal field at the interface is understood to activate the surface, thereby avoiding buildup of long-range space charge separations. The unphysical nature of this interface emerges from its large surface energy. It has been reported in several studies how isodesmic reactions whereby water hydrolysis offers hydroxide termination of surfaces and interfaces are able to drastically lower the surface energy introduced by the interface (see [9–13] again). Thus, water has two opposing roles in the corrosion process, i.e., to stabilize the surface by the hydroxylation and by acting oxygen carrier. The former contributes to the passivation of the surface, while the latter drives the corrosion.

Here, the impact of hydrolysis on stability and resulting reactivity of hydroxylated α-Al_2O_3 is explored by the slab interfaces being completely hydroxylated. Stabilization of the surface is owing to the reaction

$$\begin{cases} M_{2X}O_{3X}(\text{slab}) + H_2O(g) \rightarrow (OH)_2@M_{2X}O_{3X-1}(\text{slab}) \\ H_2O(g) + V^{\bullet\bullet}_{O,\text{surface}} + O^{x}_{O,\text{surface}} \rightarrow 2OH^{\bullet}_{O,\text{surface}} \end{cases} \quad \text{(R2)}$$

For comparison, the surface energies were computed for the fully hydroxylated surface, the half-Al/half-O, and the all-Al/all-O-terminated slabs to obtain surface energies of +0.01, +0.14, and +0.33 eV/Å^2, respectively, all relative to bulk alumina (see Fig. 4). The stabilization of the hydroxylated surface is owing to the removal of extrinsic surface states, vide infra. The low surface energy, indeed close to zero and even negative when allowing for hydrogen bonding between hydroxylated interfaces (cf. [11]), is what disfavors formation CUS owing to absence of sufficiently strong reducing agents, emphasizing the conditions for N_2 dissociation highly unlikely to be satisfied.

On Cathodic Processes at Hydroxylated Interface

The moderating impact of hydroxylation on the surface energy applies to transport properties in its vicinity as well. Indeed, both sub-surface vacancy formation enthalpies and diffusion barriers stay virtually indistinguishable as compared to the bulk values. This means to say that for the ~13-Å-thick alumina slab model employed—besides the oxygens/hydroxides in the surface—there is a sub-surface (sub) layer and a central (mid) layer for which the activation energies come out at 3.66 eV (mid) and 3.63 eV (sub) as compared to 3.66 eV (bulk). Analogously, the oxygen vacancy formation enthalpies in the yttria slab are 1.76 eV (mid) and 1.73 eV (sub) as compared to 1.77 eV (bulk). Inasmuch as mobility does not change in vicinity of the hydroxylated surface, rapid transport to satisfy the observed isotropic oxide growing defect-rich scale at the yttria/alumina interface is not realized in immediate proximity of interfaces. This leaves the equipotential at this interface to be realized by lateral hydroxylation and/or by transport of oxygen vacancies, effectively comprising hydroxide vacancies V_{OH}.

The emerging oxidation mechanism is as follows:

1. Oxygen vacancy diffusion from the alloy/oxide interface to the vicinity of the hydroxylated surface;
2. Hydroxide oxygen annihilation resulting in hydroxide proton being accommodated in the surface oxygen vacancy whereby it becomes reduced to H^-, vide infra R3
3. Any rehydroxylation of vacant surface site by hydrolysis of H_2O, whereby
   a. H_2 evolves owing to recombination of H^- with an adjacent H^+ of H_2O origin, vide infra R5
   b. Hydrogen enters sub-surface oxygen vacancies causing growth of defect-rich oxide, vide infra R8.

Indeed, maintaining oxidation through a hydroxylated surface requires disposal of the cathode product either by H_2 evolution or by incorporation of hydrogen in the oxide, at grain boundaries or in the lattice, possibly followed by transient hydrogen pickup in the alloy.

In what follows, the energetics related to the said processes is explored. Thus, introduction of an oxygen vacancy in the hydroxylated alumina surface by oxidizing aluminum displays significant exothermicity

$$\begin{cases} \frac{2}{3}Al(s) + (OH)_{12}@Al_2O_3(\text{slab}) \rightarrow \frac{1}{3}Al_2O_3(s) + (OH)_{11}H@Al_2O_3(\text{slab}) \\ V^{x}_{O} + OH^{\bullet}_{O,\text{surface}} \rightarrow O^{x}_{O} + H^{\bullet}_{O,\text{surface}} \end{cases} \quad \Delta E = -1.60 \text{ eV} \quad \text{(R3)}$$

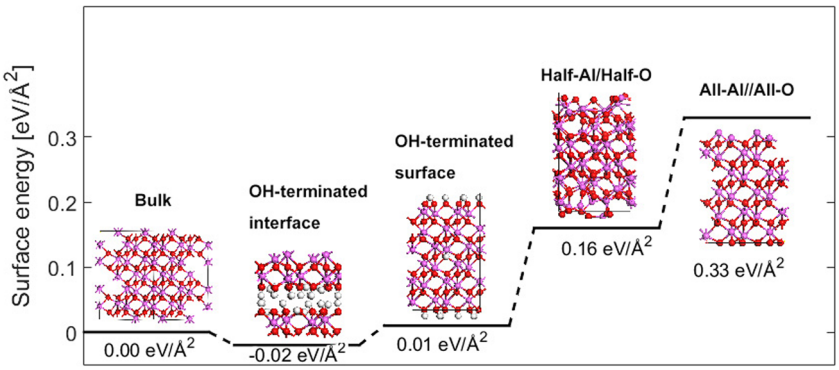

Fig. 4 Surface energies relative to bulk alumina for OH-terminated and unhydroxylated slab surfaces (see text)

It is important to recognize though that a subsequent hydrogen evolution reaction by the H^-–H^+ recombination with a vicinal proton displays significant endothermicity,

$$\begin{cases} (OH)_{11}H@Al_2O_3(slab) \rightarrow H_2(g) + (OH)_{10}O@Al_2O_3(slab) \\ H^{\bullet}_{O,surface} + OH^{\bullet}_{surface} \rightarrow V^{\bullet\bullet}_{O,surface} + O^{x}_{O,surface} + H_2(g) \end{cases} \quad \Delta E = 0.96\ \text{eV} \tag{R4}$$

This is in contrast to a H^-–H^+ recombination reaction if it occurs in consort with rehydroxylation, in case of which it comes out exothermic by

$$\begin{cases} H_2O(g) + (OH)_{11}H@Al_2O_3(slab) \rightarrow H_2(g) + (OH)_{12}@Al_2O_3(slab) \\ H_2O(g) + H^{\bullet}_{O,surface} + OH^{\bullet}_{O,surface} \rightarrow H_2(g) + 2OH^{\bullet}_{O,surface} \end{cases} \tag{R5}$$

$$\Delta E = -0.99\ \text{eV}$$

Apparently, separation of the hydrogen evolution reaction from the rehydroxylation reaction becomes prohibited. However, it is noted here that the DFT calculations underestimate the drive to oxidize aluminum by ~0.6 eV; i.e., the calculated exothermicity is 2.6 eV as compared to the experimental 3.2 eV. Taking into account the entropic contribution, assuming that $S_{1200\ K} \sim S^0 \sim$ 130 J K^{-1} mol^{-1}, renders the separate H^-–H^+ recombination reaction at 1200 K at a free hydroxylated alumina surface preferred by an additional 1.6 eV. This does not apply to the yttria/alumina or alumina/alumina interface, where a priori hydrogen evolution is mitigated owing to the confining interface suppressing H^-–H^+ recombination reaction [15, 16]. Moreover, while exothermic, it must be born in mind that concerted reactions such as R5 suggest the cathode process to be rate limiting, and it becomes difficult to see why the oxide should be rapidly growing. Two possibilities are explored here complementary to the hydrogen evolution in the grain boundary. One allows the partial deposit of hydride ions, comprising transient cathode product, in oxygen vacancies in nano-crystalline grain boundaries (see R3), and a second has hydride ions incorporated in the oxide lattice.

In order to illustrate the confinement effect, we consider here an interface between two hydroxylated alumina surfaces and compute the enthalpy of effusion to obtain

$$H_2(GB) \rightarrow H_2(g) \quad \Delta E = -1.75\ \text{eV} \tag{R6}$$

For the H_2(GB), see Fig. 5. Thus, by virtue of R5, we arrive at

$$H_2O(g) + (OH)_{11}H@Al_2O_3(slab) \rightarrow H_2(GB) + (OH)_{12}@Al_2O_3(slab) \quad \Delta E = 0.76\ \text{eV} \tag{R7}$$

Hence, it is conceivable that the effective cathode surface at said interface at steady state constitutes, besides the mainly hydroxylated alumina interface, also $H^-@V_{OH}$

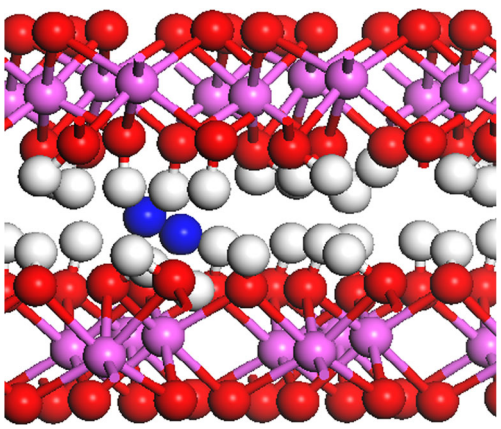

Fig. 5 Local character of model of hydroxylated interface between alumina grains. The interface contains a H_2 molecule. Oxygen is in *red* and aluminum in *purple*. Hydrogen is in *white* except for the H_2 molecule, which is in *blue*

moieties owing to the confining surrounding. Existence of interface V_{OH} sites per se is unlikely at steady state.

On Rapid Alumina Growth Below Yttria-Rich Nodules

Experiments exhibit rapid inward alumina growth in the vicinity of the irregular yttria-rich nodules (see Fig. 1). The resulting alumina scale displaying hemispheric uniform thickness is taken to imply that the yttria/alumina interface must exhibit an electrochemical equipotential in oxygen. This in conjunction with the rapidly growing alumina scale not comprising α-alumina is understood to mean deliverance of oxygen into the yttria/alumina interface to be much faster than the depletion at this interface owing to the process of oxide growth. This can be achieved in two ways, first by considering that oxygen diffusion is rapid in grain boundaries and interfaces and especially so when decorated by reactive elements such as yttrium. The other possibility is the quicker oxygen diffusion in yttria particles (Q^{bulk}_{Y2O3}≈2.5 eV). Oxygen vacancies would be formed at the metal/oxide interface following reaction R1, diffuse to the hydroxylated yttria/alumina interface, where the oxygen of water origin would act as a sink for the oxygen vacancies rendering these annihilated. It becomes apparent, however, that the enthalpy cost for transfer of such vacancies into bulk yttria is prohibitively high in spite of the fact that the subsequent activation energy for diffusion is low when compared to alumina. This is in contrast to the high mobility offered by the alumina/yttria interface, in particular as this transport benefits naturally from the reactive element effect. This suggests that the equipotential along the yttria/alumina interface is maintained by lateral hydrolysis-driven diffusion. This emphasizes the role of $H^{\cdot}_{O,surface}$ as cathode product discussed in the "On Cathodic Processes at Hydroxylated Interface" section and possibly also incorporation of $H^{\cdot}_{O}$ in the alumina lattice consistent with inward growth of a disordered alumina scale. Indeed, a possible straightforward cause for rapid alumina growth below the yttria-rich nodules emerges, comprising accommodation of hydride ions by inward diffusion through the alumina scale by utilizing the oxygen vacancies building on reactions of the form

$$\begin{cases} H_2O(g) + (OH)_{11}H@Al_2O_3(V_O)_2(slab) \rightarrow (OH)_{12}@Al_2O_3(H@V_O)_2(slab) \\ H_2O(g) + H^{\bullet}_{O,surface} + OH^{\bullet}_{O,surface} + 2V^{x}_{O} \rightarrow 2OH^{\bullet}_{O,surface} + 2H^{'}_{O} \end{cases} \Delta E = -0.26\ \text{eV} \quad \text{(R8)}$$

It is tempting to conclude that this channel for disposing the cathode product, i.e., by utilizing the oxygen vacancies, is indeed exothermic as well as superior to hydrogen evolution channel when taking into account that the latter suffers from the confining condition of the cathode as set by the yttria/alumina interface (cf. $\Delta E = +0.78$ eV in R7). Such transient incorporation of hydrogen into oxygen vacancies of the growing alumina scale is what would render it rapidly growing, i.e., by offering an alternative to the hydrogen evolution condition for sustained oxidation by water. However, it is noted that incorporation of hydrogen in the interior of the hydroxylated alumina slab renders the extrinsic surface band occupied. Inasmuch as GGA underestimates the band gap owing to the self-interaction energy, the favorable reaction R8 must be met with great caution. It is gratifying to note that upon closing the vacuum slab allowing the hydroxylated interfaces to form the hydroxylated grain boundary, the band gap increases rendering the incorporation of cathode product in the lattice inaccessible. Characteristic features of the oxygen vacancy are displayed in Fig. 6, while the impact of hydrogen accommodation is shown in Fig. 7.

$$\begin{cases} H_2O(g) + (OH)_{11}H@Al_2O_3(V_O)_2(GB) \rightarrow (OH)_{12}@Al_2O_3(H@V_O)_2(GB) \\ H_2O(g) + H^{\bullet}_{O,surface} + OH^{\bullet}_{O,surface} + 2V^{x}_{O} \rightarrow 2OH^{\bullet}_{O,surface} + 2H^{'}_{O} \end{cases} \Delta E = +1.47\ \text{eV} \quad \text{(R9)}$$

A difference of approximately 1.5 eV reflects well the increase in band gap (cf. Figs. 7c and 8c). Hydride incorporation is not accessible in the interface in the same extent as on the surface. Figure 7b,c shows the nature of the HOMO and how it ends up in the conduction band. In contrast, Fig. 8 depicts the properties of the freestanding hydroxylated slab. Indeed, the fact that the valence band is full forces the excess electrons to occupy the extrinsic surface state. Moreover, it is noted that the splitting between valence and conduction bands increases from ~4.5 eV for freestanding slab (see Fig. 8c) to ~6 eV when allowing for hydrogen bonding between hydroxylated interfaces (see Fig. 7c). Thus, there is no driving force to incorporate hydrides into the matrix, and if hydrides are to be found, they are to be found at interfaces and grain boundaries.

Hence, suppression of the hydrogen evolution channel under yttria-rich nodules disfavors formation of the slow-growing α-Al_2O_3 barrier oxide. Instead, formation of rapidly growing defect-rich, non-protective alumina scale is observed. This does not necessarily mean that α-Al_2O_3 is not formed but

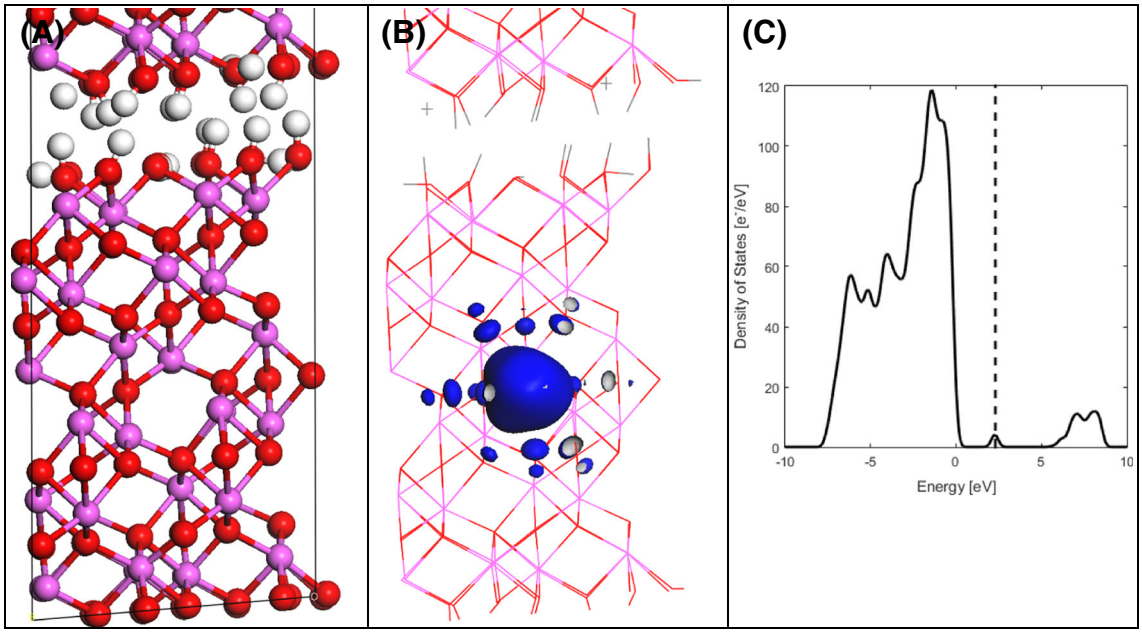

Fig. 6 **a** Hydroxylated interface slab model that is shown including an oxygen vacancy in the alumina matrix is depicted. **b** Highest occupied molecular orbital (HOMO) seen to reside in the oxygen vacancy site. **c** DOS showing the HOMO in **b** to comprise an impurity state in the band gap

rather that it stays granular owing to partial hydroxide, partial hydride termination of the grain boundaries. It is noted that such proton reduction causes transient buildup of negative space charge at the grain boundaries, suggestive of inward drag of protons as well as other cations.

A possible context offered for the oxidation process comprises hydroxylated nano-crystalline grain boundaries, mediating the oxygen all the way to the metal/oxide interface. In order to sustain this oxidation process, hydrogen pickup in the alloy is understood to offer an alternative means for transient disposal of hydrogen other than hydride ion accommodations in oxygen vacancies at grain boundaries, both competing with the hydrogen evolution reaction in the confined surroundings offered by the hydroxylated grain boundaries.

Electronic Structure Considerations

For completeness, it becomes interesting to understand how hydroxylation impacts the resulting electronic structure and in turn also the surface energy of the slab model. To this end,

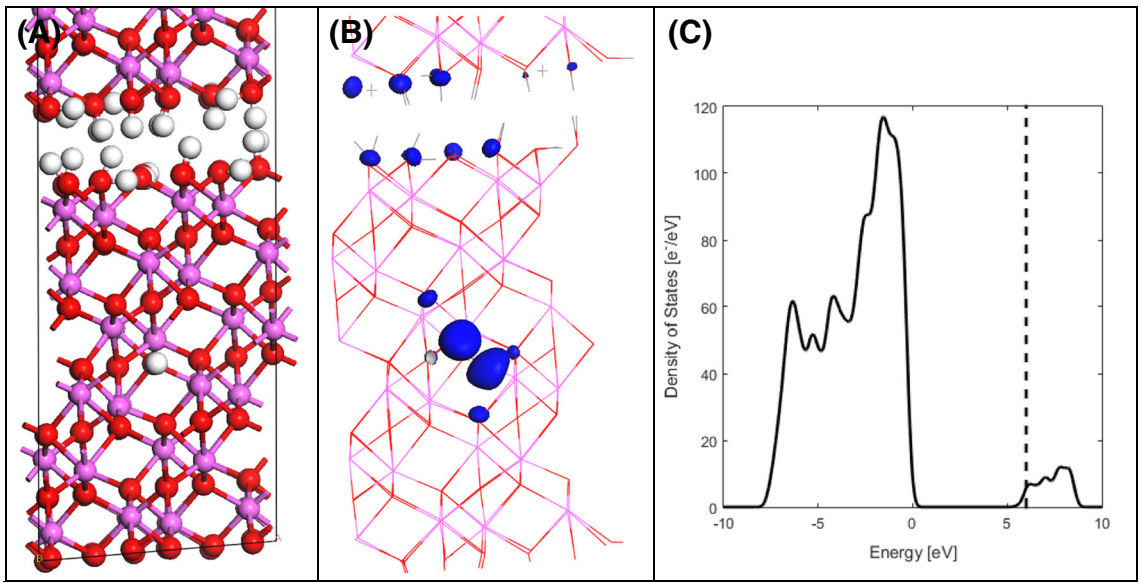

Fig. 7 **a** Hydroxylated grain boundary model is shown including a hydride ion residing in an oxygen vacancy in the alumina matrix. **b** Highest occupied molecular orbital (HOMO) distributed between surface states and vacancy site. **c** The HOMO is seen to reside in the extrinsic conduction band found ~6 eV above the valence band

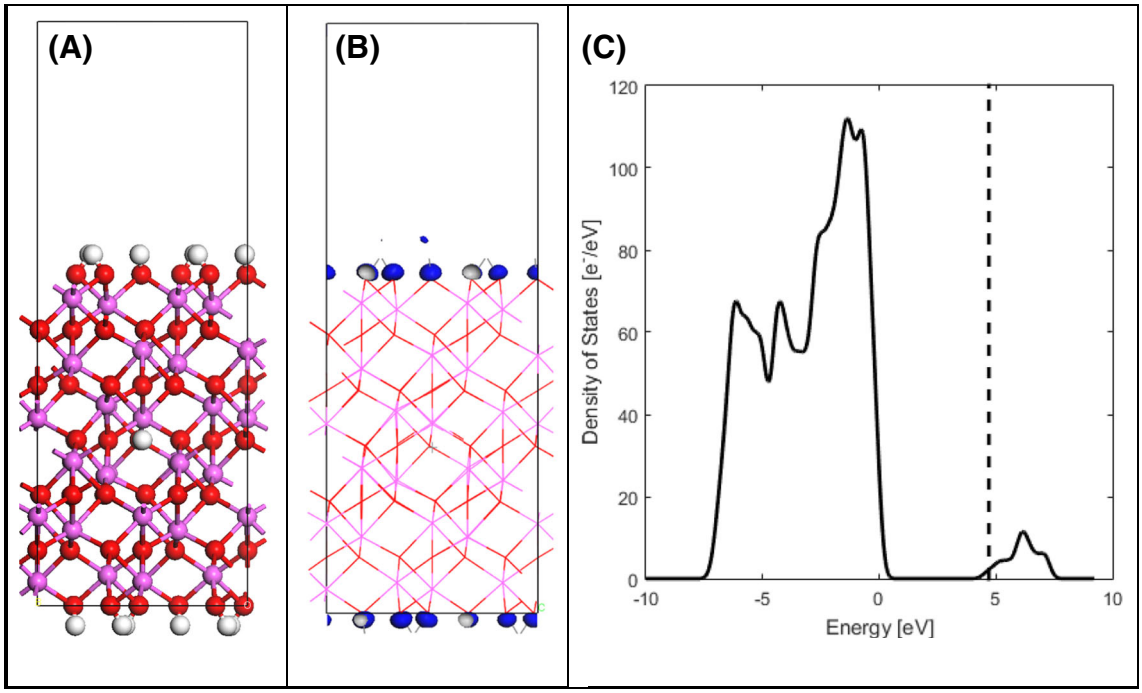

Fig. 8 **a** Hydroxylated freestanding slab model is shown including a hydride ion residing in an oxygen vacancy in the alumina matrix. **b** Highest occupied molecular orbital (HOMO) utilizing surface states only. **c** The HOMO is seen to reside in the conduction band comprising extrinsic surface states ~4.5 eV above the valence band

compare the density of states of all-Al//all-O and half-Al/half-O-terminated slabs to those of the hydroxylated slab and to α-alumina bulk. Incomplete screening of the Coulombic repulsion among outer oxygen ions renders the local Al-O bonds increasingly covalent, thus causing the gap size to diminish and even close (see Fig. 9). Indeed, the all-Al//all-O slab can be seen to have no band gap at the Fermi level, which implies that the slab surface is electronically conducting. The densities

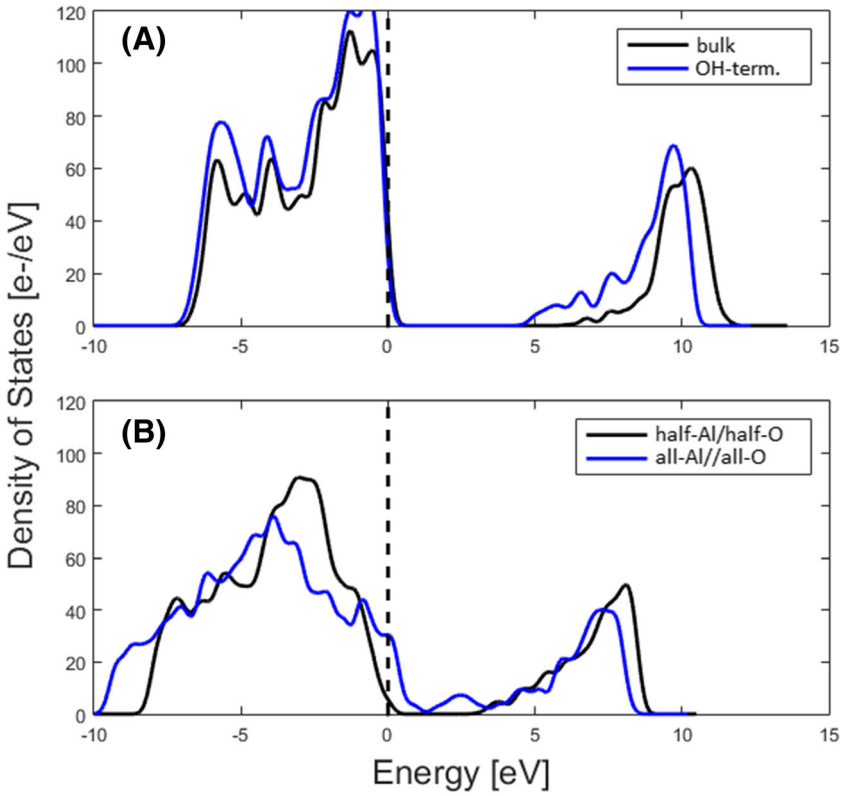

Fig. 9 Density of states (DOS) plotted against energy for **a** bulk alumina is compared to OH-terminated alumina slab, and **b** all-Al//all-O and half-Al/half-O-terminated slabs are compared. The *dotted line* shows the Fermi energy

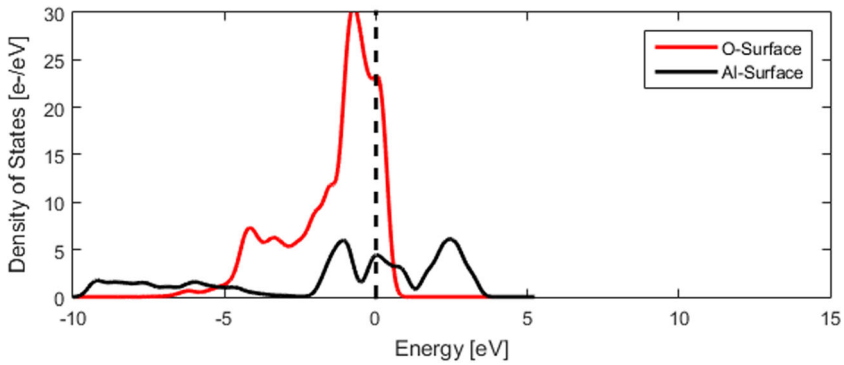

Fig. 10 Density of states for the two terminal surface layers in the all-Al//all-O slab (cf. Fig. 2). While both being metallic, they possess electron-like (Al terminated) and hole-like (O terminated) carriers at the two interfaces

of states of the surface oxygen-terminated and aluminum-terminated interfaces, shown in Fig. 10, display hole and electron conduction, respectively. This is taken to imply that indeed, the metal-terminated surface hosts electrons potentially able to support N_2 dissociation. The artificial nature of this termination of an alumina surface in conjunction with the ability to only partly dissociate the N-N bond was employed in [7] to contrast the reduced chromia surface, which readily dissociates the N-N bond.

Improved screening of Coulomb repulsion at the alumina surface is achieved upon hydrolysis. Thus, the protons pull the top of the valence band associated with the surface atoms to coincide with the bulk states (see Fig. 9a). Interestingly, the position of the conduction band is not affected, implying that the polar covalent Al-O contribution is not changed upon hydrolysis but only the ionic repulsion among surface oxygens. Moreover, it was observed above that the activation energy for oxygen vacancy diffusion in the hydroxylated slab does not differ significantly from that in bulk alumina. Considering Fig. 9b where we see a smaller band gap (~3 eV) compared to bulk alumina (~7–9 eV) in the case of half-Al/half-O, we may ask if this can be exploited by the oxygen vacancy diffusion, i.e., in order to lower the activation energy by transferring electrons from the vacancy to the surface states at the transition state. Our simulations show, however, that even though the band gap has diminished significantly, the vacancy states at the transition state are not sufficiently destabilized to access the states at the bottom of the conduction band. The inability of extrinsic states to act transient sinks for electrons, complementary to hydrogen reduction, clarifies the importance of $H^{\cdot}_{O,surface}$ and $H^{\cdot}_{O}$ comprising concerted deposits of both protons and electrons. The dramatic lowering of the activation energy for oxygen vacancy diffusion when being oxidized is repeatedly emphasized [12, 27, 28].

Concluding Remarks

Possible factors controlling rapid growth of non-protective aluminum oxide below yttria nodules upon oxidation of FeCrAl(Y) alloy at a 95% N_2/5% H_2/~35 ppm H_2O at 1200 K were explored. First-principle modeling in a quasi-Wagnerian context was employed to unravel discriminating factors viz. nitridation. The inward growing oxide, displaying hemispheric uniform thickness, was taken to offer an essential clue to this behavior. Dual-transient fates of hydrogen emerged as decisive. Thus,

- Oxygen vacancy formations in alpha-alumina as well as in yttria are highly endothermic processes offering a rationale for (a) formation of defect-rich alumina as a condition for rapid growth and (b) suggesting a passive (non-redox active) role of the yttria particle besides that of introducing a wedge, providing a confining boundary to the growing defect-rich alumina scale, as well as non-healing interfaces.
- Extrinsic electronic states owing to various surface oxide terminations did not markedly change the mobility of oxygen vacancies in the vicinity of the interface.
- Stabilization of the interface by hydrolysis was demonstrated.
- High stability of the interface and low activation energies based on Grotthuus mechanism for the hydrolysis-mediated process were proposed to explain the constant oxygen activity along the yttria/alumina interface offering a robust boundary condition for the inward alumina growth.
- Moreover, the efficient surface termination offered by the hydroxylation was taken to (a) violate necessary requirement for N_2 dissociation comprising extended domains coordinatively unsaturated metal site CUSs at the yttria/alumina interface and (b) disconnect any oxygen vacancy transport through the yttria particle and hence disallow formation of CUS domains on the outer yttria surface repeatedly required for any N_2 dissociation.
- The efficient process of alumina growth competing for aluminum atoms with the internal nitridation—the latter owing to chromia particles acting windows for nitrogen pickup—suggests new strategies analogous to pre-oxidation to improve the corrosion resistance of FeCrAl.
- Dual fates of the hydrogen produced in the cathode process, i.e., H_2 evolution and H^{-} incorporation in oxygen vacancies at hydroxylated grain boundaries, are suggested.

The last point in particular is understood to facilitate rapid growth of alumina, rich with hydroxylated interfaces. This is owing to hydrides residing in oxygen vacancies offering alternative means to deposit cathode products, as the H_2 evolution reaction becomes suppressed due to the confining hydroxylated yttria/alumina and alumina/alumina interfaces. It is repeatedly noted that thin virtually, defect-free α-Al_2O_3 barrier oxide is formed in absence of the constraining confinement.

Acknowledgements This work was carried out within the Swedish High Temperature Corrosion Centre (HTC) and was supported by Sandvik Heating Technology AB. Assistance by Nooshin Mortazavi in acquiring the SEM images is acknowledged. The Swedish Research Council is gratefully acknowledged for the financial support.

References

1. T. Norby, M. Wideroe, R. Glöckner, Y. Larring, Hydrogen in oxides. Dalton Trans. **19**, 3012–3018 (2004)
2. C. Wagner, Equations for transport in solid oxides and sulfides of transition metals. Prog. Solid State Chem. **10**, 3–16 (1975)
3. C. Wagner, Beitrag zur Theorie des Anlaufvorgangs. Z. Phys. Chem. B **21**, 25–41 (1933)
4. C. Wagner, Diffusion and high-temperature oxidation of metals in: Atom Movements, American Society of Metals, Cleveland, 1951, pp. 153–173
5. P. Kofstad, Growth of oxide scales by lattice transport in: High temperature corrosion, Elsevier Applied Science Publishers LTD, Essex, 1988, pp. 162.
6. P. Alnegren, M. Sattari, J.-E. Svensson, J. Froitzheim, Severe dual atmosphere effect at 600 °C for stainless steel 441. J. Power Sources **301**, 170–178 (2016)
7. C. Geers et al., Properties of alumina/chromia scales in N_2-containing low oxygen activity environment investigated by experiment and theory. Oxid. Met. (2017). doi:10.1007/s11085-016-9703-3
8. V. Kochubey et al., Effects of minor additions and impurities on oxidation behavior of FeCrAl alloys. Development of novel surface coatings compositions. Mater. Corros. **56**(12), 848–853 (2005)
9. P.J. Eng, T.P. Trainor, G.E. Brown Jr., G.A. Waychunas, M. Newville, S.R. Sutton, M.L. Rivers, Structure of the hydrated α-Al_2O_3 (0001) surface. Science **288**(5468), 1029–1033 (2000)
10. J.M. McHale, A. Auroux, A.J. Perrotta, A. Navrotsky, Surface energies and thermodynamic phase stability in nanocrystalline aluminas. Science **277**(5327), 788–791 (1997)
11. X.G. Wang, A. Chaka, M. Scheffler, Effect of the environment on α-Al_2O_3 (0001) surface structures. Phys. Rev. Lett. **84**, 3650–3653 (2000)
12. Z. Lodziana, N.-Y. Topsøe, J.K. Nørskov, A negative surface energy for alumina. Nat. Mater. **3**, 289–293 (2004)
13. R.B. Bagwell, G.L. Messing, Effect of seeding and water vapor on the nucleation and growth of α-Al_2O_3 from γ-Al_2O_3. J. Am. Ceram. Soc. **82**(4), 825–832 (1999)
14. V. Babic, C. Geers, B. Jonsson, J-E. Svensson, L-G. Johansson, I. Panas, Effects on oxygen vacancy diffusivity of substitutional 3D elements doping in alpha-alumina, Oxidation of Metals, submitted (2017)
15. M. Lindgren, I. Panas, Confinement dependence of electrocatalysts for hydrogen evolution from water splitting. Beilstein Journal of Nanotechnology **5**, 195–201 (2014)
16. M. Lindgren, I. Panas, Impact of additives on zirconium oxidation by water: mechanistic insights from first principles. RSC Adv. **3**, 21613–21619 (2013)
17. M.A. Monge, R. González, A.I. Popov, R. Pareja, Y. Chen, E.A. Kotomin, M.M. Kuklja, The dynamics of the hydride ion in MgO single crystals. Defect and Diffusion Forum **169–170**, 1–11 (1999)
18. P. Hohenberg, W. Kohn, Inhomogeneous electron gas. Phys. Rev. B **136**, B864–B871 (1964)
19. W. Kohn, L.J. Sham, Self-consistent equations including exchange and correlation effects. Phys. Rev. **140**, A1133–A1138 (1965)
20. D. Vanderbilt, Soft self-consistent pseudopotentials in a generalized eigenvalue formalism. Phys. Rev. B **41**, 7892–7895 (1990)
21. J.P. Perdew, K. Burke, M. Ernzerhof, Generalized gradient approximation made simple. Phys. Rev. Lett. **77**, 3865–3868 (1996)
22. S.J. Clark, M.D. Segall, C.J. Pickard, P.J. Hasnip, M.J. Probert, K. Refson, M.C. Payne, First principles methods using CASTEP. Zeitschrift Fur Kristallographie **220**, 567–570 (2005)
23. H.J. Monkhorst, J.D. Pack, Special points for brillouin-zone integrations. Phys. Rev. B **13**, 5188–5192 (1976)
24. Materials Studio 6.0, in, Accelrys Inc., pp. Simulation software
25. M. Lindgren, I. Panas, On the fate of hydrogen during zirconium oxidation by water: effect of oxygen dissolution in α-Zr. RSC Adv. **4**, 11050–11058 (2014)
26. M. Lindgren, I. Panas, Oxygen vacancy formation, mobility and hydrogen pick-up during oxidation of zirconium by water. Oxid. Met. (2016). doi:10.1007/s11085-016-9695-z
27. M.Y. Yang et al., Charge-dependent oxygen vacancy diffusion in Al_2O_3-based resistive-random-access-memories. Appl. Phys. Lett. **103**(9), 093504 (2013)
28. M. Lindgren, C. Geers, I. Panas, Oxidation of Zr alloys by water—theory from first principles, Corrosion Science, submitted (2017)